

Highly Efficient Charge Separation and Collection across in Situ Doped Axial VLS-Grown Si Nanowire p–n Junctions

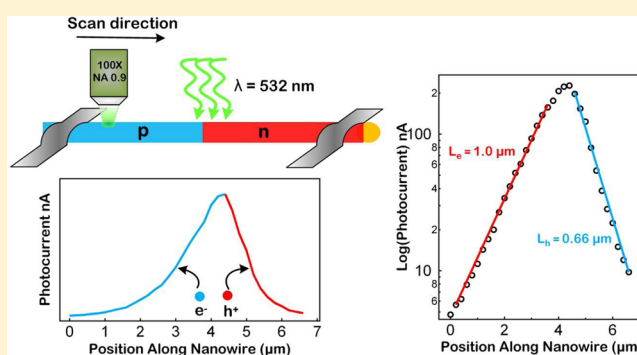
A. D. Mohite,^{*,†,§} D. E. Perea,^{†,‡,||} S. Singh,^{†,§,⊥} S. A. Dayeh,^{†,‡} I. H. Campbell,[‡] S. T. Picraux,^{*,†,‡} and H. Htoon^{*,†,§}

[†]Center for Integrated Nanotechnologies, [‡]Material Physics and Applications Division, and [§]Chemistry Division, Los Alamos National Laboratory, Los Alamos, New Mexico 87544, United States

S Supporting Information

ABSTRACT: VLS-grown semiconductor nanowires have emerged as a viable prospect for future solar-based energy applications. In this paper, we report highly efficient charge separation and collection across in situ doped Si p–n junction nanowires with a diameter <100 nm grown in a cold wall CVD reactor. Our photoexcitation measurements indicate an internal quantum efficiency of ~50%, whereas scanning photocurrent microscopy measurements reveal effective minority carrier diffusion lengths of ~1.0 μm for electrons and 0.66 μm for holes for as-grown Si nanowires ($d_{\text{NW}} \approx 65\text{--}80\text{ nm}$), which are an order of magnitude larger than those previously reported for nanowires of similar diameter. Further analysis reveals that the strong suppression of surface recombination is mainly responsible for these relatively long diffusion lengths, with surface recombination velocities (S) calculated to be 2 orders of magnitude lower than found previously for as-grown nanowires, all of which used hot wall reactors. The degree of surface passivation achieved in our as-grown nanowires is comparable to or better than that achieved for nanowires in prior studies at significantly larger diameters. We suggest that the dramatically improved surface recombination velocities may result from the reduced sidewall reactions and deposition in our cold wall CVD reactor.

KEYWORDS: *Minority carrier diffusion length, photocurrent, p–n junction, nanowire, scanning photocurrent microscopy*



Silicon (Si) is an excellent material for solar energy applications as it offers a near ideal band gap for conversion of solar photons to electricity and is also widely abundant. However, the high cost of producing high purity wafers for single crystalline cells and the lower efficiency for polycrystalline and amorphous thin film cells has restricted the more widespread use of silicon-based photovoltaic technology^{1–3} and has promoted research for alternative nonplanar based Si cells such as Si nanowire (NW) solar cells.^{4–12} Silicon NWs grown by the vapor–liquid–solid (VLS) process¹³ offer distinct advantages for use in solar cells, including a reduced amount of Si material, control over the diameter and aspect ratio¹⁴ for enhanced optical absorption,^{9,11,15} ability to fabricate axial¹⁶ and radial p–n junction devices,^{17,18} and in situ incorporation of dopants.¹⁹ However the overall efficiency of photovoltaic devices fabricated to date from Si NW arrays has been limited to ~7.9%, which is still far from predicted maximum values and much less than the 15–20% efficiency desired for commercial viability.²⁰ A better understanding and control over the competition between charge recombination and charge separation/collection processes in these NWs is essential for designing more efficient Si NW solar cells.

The recombination of photogenerated minority carriers occurs mainly via dopants and a variety of crystalline defects

which limits the charge separation and collection efficiency in bulk Si. In addition, minority carrier recombination in VLS grown NWs is expected to be further increased by the unintentional incorporation of metallic impurities from the growth catalysts (e.g., Au),²¹ as well as the increased influence of the relatively large proportion of unpassivated surface states.¹⁵ The efficiency of the separation and collection of photogenerated carriers can be measured by the average distance or time a photogenerated carrier can travel before recombination, i.e., minority carrier diffusion length, L , or lifetime, τ , which are related to one another by $L = (D\tau)^{1/2}$, where D is the carrier diffusion coefficient.²² In addition, the surface recombination velocity, S , provides a measure of the degree of surface passivation without the influence of dopant concentration or the increased surface to volume ratio with decreasing NW diameter. Experiments to date have applied electron beam induced current (EBIC)²³ or scanning photocurrent microscopy (SPCM)^{24–26} to measure the effective minority carrier diffusion lengths (L^{eff}) across Schottky junctions of doped nano or microscale wires or ex situ doped

Received: December 21, 2011

Revised: March 6, 2012

Published: March 20, 2012

p–n junctions of micropillars. These studies have revealed that L^{eff} values scale with the NW diameter. More importantly, they also revealed a dramatic increase in L^{eff} by surface passivation via several different approaches such as with hydrogen termination or silicon nitride,²⁶ thin amorphous Si layer coatings,²⁴ or via background illumination.²⁷ These findings provide clear evidence that the recombination of photo-generated carriers at unpassivated surface states plays a dominant role in limiting the efficiency of the charge separation and collection processes. The ability to control the quality of the surface with CVD growth conditions and processing parameters therefore holds the key to achieving high performance NW-based solar photovoltaics.

In this letter, we describe the first report on measuring both the electron and hole effective minority carrier diffusion lengths in in situ doped, Au catalyzed small diameter (<100 nm) axial p–n junction Si NWs. In contrast to the Si NWs grown by the VLS method by previous groups using hot wall reactors, these p–n junction NWs were grown using a cold wall reactor in a hydrogen rich environment. This could significantly alter the reactivity of the precursor gases, for example minimizing NW sidewall reactions and deposition, and result in surfaces with a lower density of unpassivated surface states compared to those grown in hot wall reactors. Indeed, we observed that L^{eff} for both the electrons and holes in our as-grown NWs are an order of magnitude longer than those previously reported on similar diameter Si NWs,²³ and even longer than was achieved after passivation with a thin amorphous Si layer.²⁴ Furthermore, we also observed that background light illumination, which was previously shown to optically passivate surface states and give rise to a dramatic increase in L^{eff} of hot wall reactor grown microwires,²⁷ has no effect on our NWs. On the basis of these observations, we suggest that the density of surface states in NWs grown using a cold wall CVD reactor can be significantly lowered compared to hot-wall reactor growth.

The cold wall CVD reactor growth of silicon p–n junction NWs used for this study employed SiH_4 as the Si source precursor and H_2 as the carrier gas. The NWs were grown using the VLS growth technique from a 2 nm thick UHV electron beam evaporated Au film deposited on a solvent cleaned and dilute HF etched and passivated Si(111) substrate²⁸ that was initially solvent cleaned and native oxide etched. Nanowire growth was initiated at 550 °C by simultaneously flowing 300 and 10 sccm of SiH_4 (50% in H_2) and B_2H_6 (100 ppm in H_2), respectively. After 2 min of growth of the B-doped Si segment, a P-doped segment was grown by simultaneously stopping the B_2H_6 flow and introducing PH_3 (100 ppm in H_2) at 100 sccm for 3.5 min while maintaining a 300 sccm SiH_4 flow. A total pressure of 3 Torr was maintained throughout the growth. The growth times were chosen such that the resulting NW lengths were $\sim 15 \mu\text{m}$ with the p–n junction at the center of the NW. Devices were fabricated from individual NWs by first drop casting NWs suspended in isopropyl alcohol onto a 100 nm thick oxide layer on a degenerately doped Si substrate. The NW locations were mapped using an optical microscope, and electron beam lithography was used to define the contact areas. E-beam evaporation was then used to deposit 120 nm thick Ni contacts on both the B-doped and P-doped Si segments. Figure 1a shows a schematic of the device structure and an optical image of the actual device used for our SPCM measurements.

Figure 1b shows the current–voltage characteristics of a two terminal p–n diode device in the dark measurement (red curve) and under illumination (green curve). Upon optical

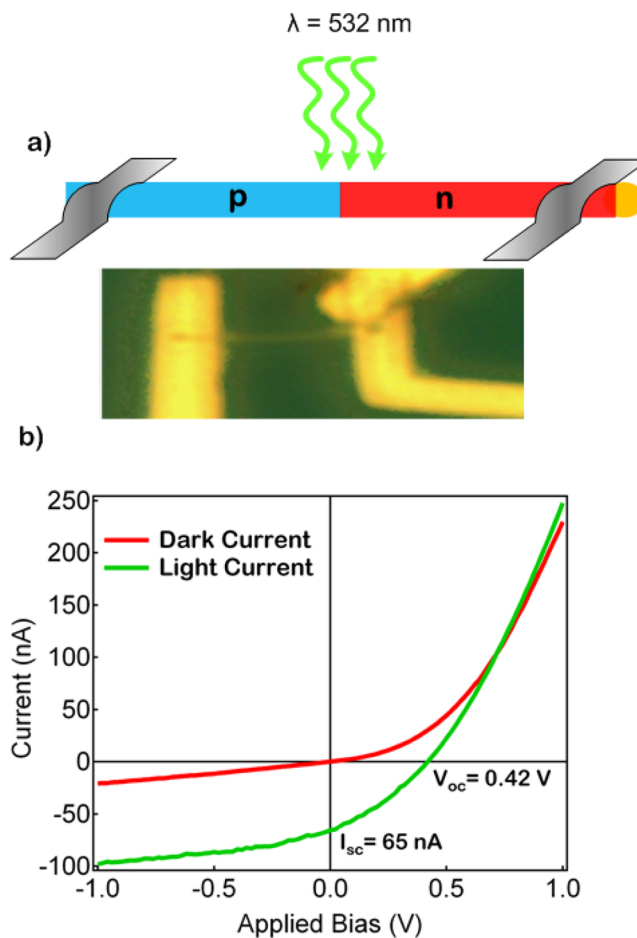


Figure 1. (a) Schematic of the axial p–n junction device and an optical image of the actual device with ohmic contacts. (b) Current voltage curve measured in the dark (red) and under illumination (green) with 532 nm excitation wavelength shows typical solar cell response.

excitation of the p–n junction with a green diode pumped solid state laser ($\lambda = 532 \text{ nm}$) coupled through a confocal microscope, a typical photovoltaic response is observed with $V_{\text{oc}} = 0.42 \text{ V}$ and $I_{\text{sc}} = 65 \text{ nA}$ (green curve). We estimate an internal quantum efficiency (IQE) of $\sim 50\%$ at zero bias for illumination with monochromatic light of $\lambda = 532 \text{ nm}$, a NW diameter = 80 nm, laser spot size $\sim 500 \text{ nm}$, incident power = $100 \mu\text{W}$, absorption coefficient = 10^4 cm^{-1} , and a reflection coefficient = 0.35. The magnitude of the IQE suggests that the NW p–n junction exhibits strong photosensitivity, indicating good crystalline quality and photovoltaic properties.

Through analysis of the spatial variation in the locally excited photogenerated electron–hole pairs measured by SPCM we determine (1) the nature of the contacts (ohmic or Schottky), (2) individual segment electrical type (p or n), and (3) the minority carrier diffusion lengths in our in situ doped Si p–n junction NWs. A schematic of the experimental setup for the measurement of the L^{eff} is illustrated in Figure 2a. A modulated green laser was coupled through a confocal microscope to obtain a diffraction limited laser spot which was scanned over a distance of approximately $6 \mu\text{m}$ between the two electrodes of the two terminal device in the direction from the p-doped region to the n-doped region of the NW, while measuring the photocurrent in 200 nm steps. At each position the photocurrent was measured as a function of applied bias which was scanned from +1 to -1 V with 0.1 V increments.

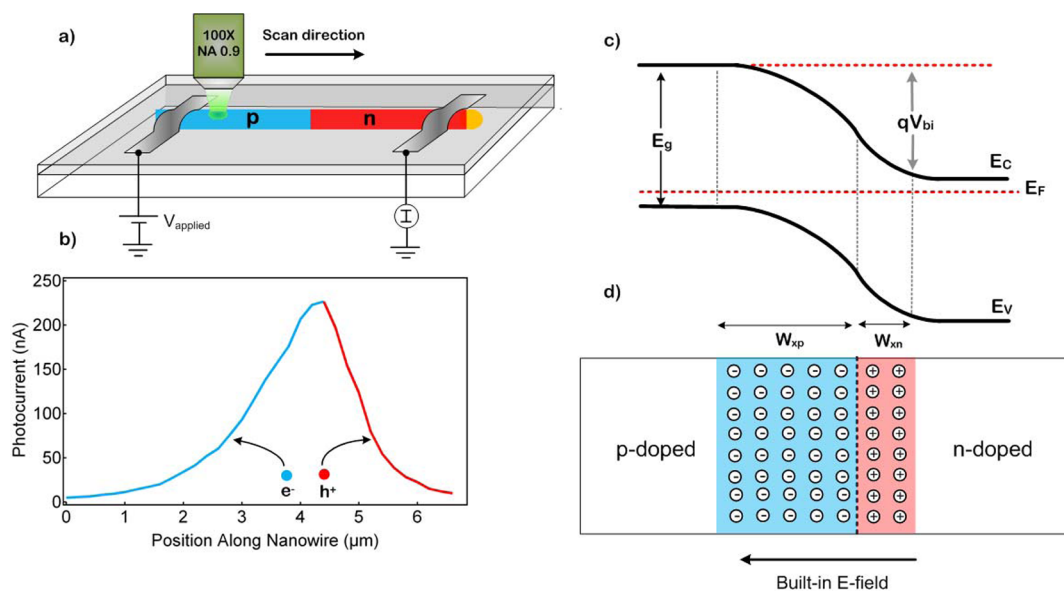


Figure 2. (a) Experimental setup for SPCM measurements. Laser is scanned along the nanowire and photocurrent is collected as a function of applied dc bias. (b) Photocurrent profile along the length of the nanowire with blue half of the curve representing electron transport and red represents hole transport. (c) Schematic of the band diagram depicting a graded p–n⁺ junction with majority of the depletion region on the p-doped segment of the nanowire, and (d) corresponding space-charge region in the device.

The photocurrent was collected using a lock-in amplifier synched at the modulation frequency of the incident laser (513 Hz). Figure 2b shows the photocurrent versus the position along the NW axis for the case of 0 V applied bias. A peak in the photocurrent is observed at a position corresponding to approximately the middle of the NW, consistent with the intended location of the p–n junction determined from the growth rate and sequence of the exposed dopants gases flown. As prior studies have reported high photocurrent near Schottky contacts,²³ our observation of a very small photocurrent near the contacts for our devices provides a clear indication of net ohmic contact behavior. As an additional check we also examined the case where we formed metal–NW Schottky contacts and observed higher photocurrents near the NW–metal contact as compared to the magnitude of the photocurrent at the p–n junction near the center of the NW device. From the polarity of the current flow, the known growth sequence and the direction of taper in the NW, we can unambiguously identify each of the p and n segments. The approximate doping concentrations in the boron doped p- and phosphorus-doped n segments were determined by standard four probe resistivity measurements performed separately on each segment of the NW grown in the same batch as the one discussed here. Under the assumption of bulk mobility values we obtain $N_A \sim 2 \times 10^{16} \text{ cm}^{-3}$ for holes and $N_D \sim 2 \times 10^{18} \text{ cm}^{-3}$ for electrons, indicating a p–n⁺ doping sequence for our axial NW junctions.

The peak in the photocurrent signal corresponds to the geometric center of the depletion region (see Figure 2b), with the photocurrent expected to decay exponentially on either side. To understand this, consider the schematic band diagram shown in Figure 2c and corresponding space charge region in Figure 2d representing a graded p–n⁺ junction with the larger depletion width on the p side of the junction. The charge collection probability is maximum when the electron–hole pairs are generated inside or within a diffusion length of the depletion region where they are separated by the built-in

electric field and drift toward their respective contacts to generate a photocurrent. Upon moving away from the depletion region, the collection probability and thus the photocurrent decays exponentially with distance, with different decay rates for electrons and holes. Beyond a distance of one diffusion length, the generated minority carriers have a higher probability to recombine with the majority carriers of opposite polarity than to be collected.

The measured L^{eff} for both electrons and holes within the in situ doped p–n junction nanowires described here are an order of magnitude greater than previously reported for similar diameters. Figure 3a shows the semi log plot of the photocurrent at 0 V applied bias (open circles) for a p–n junction NW of diameter 70 nm. The vertical dashed lines mark the edge of the hole (blue) and electron (red) collector contacts. The effective minority carrier diffusion length for electrons (L_e^{eff}) and holes (L_h^{eff}) was extracted by fitting the exponential decay of the photocurrent to the equation $I = I_0 \exp(\pm(x-d)/L_{e,h}^{\text{eff}})$, as described previously by Gu et al.²⁹ Here we find a good fit and determine a value of $L_e^{\text{eff}} \approx 1.0 \mu\text{m}$ for electrons and $L_h^{\text{eff}} \approx 0.66 \mu\text{m}$ for holes. As an additional check on these surprisingly long $L_{e,h}^{\text{eff}}$ in Si NWs, we performed SPCM measurements on a n-type NW segment for which a Schottky barrier contact with Ni was formed.³⁰ As seen in Figure 3b, the photocurrent versus position shows a maximum photocurrent at the contact position (vertical dashed line) where the photogenerated electron–hole pairs are separated by the depletion region formed between the NW and the Ni contact. A fit to the exponential decay in this case gives $L_h^{\text{eff}} \approx 0.64 \mu\text{m}$ for the NW with $d \approx 70 \text{ nm}$, in good agreement with the results obtained for the p–n junction devices. In order to eliminate the possibility of the measured diffusion lengths being limited by the spatial resolution of the SPCM measurement, other control experiments included using a smaller excitation spot size, as well as making SPCM scans perpendicular to the NW length were performed and can be found in the Supporting Information.

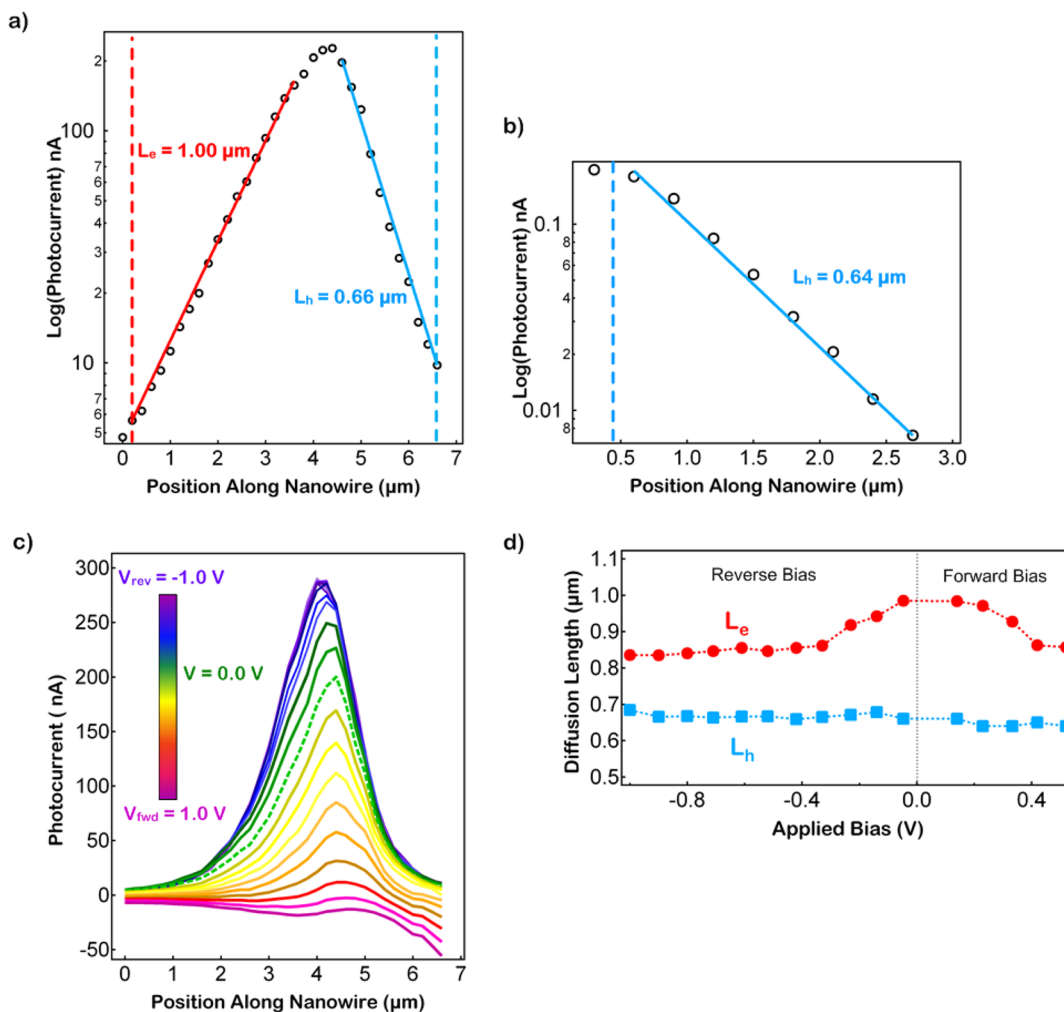


Figure 3. (a) Semi log plot of the photocurrent profile for the Si nanowire p–n junction measured at 0 V. The red and blue solid lines are exponential fits to obtain the effective electron and hole diffusion lengths. The dotted vertical lines mark the inner edge of the contacts. (b) Semi log plot of the photocurrent profile for a Schottky barrier device contacting an n-type segment measured at 0 V. The dotted line represents the inner edge of the Schottky contact. (c) Photocurrent plotted as a function of position along nanowire for the applied dc bias stepped from +1 V forward bias to –1 V reverse bias. The magnitude of photocurrent is represented by the rainbow scale. The dotted green line shows the photocurrent profile measured at 0 V. (d) Effective minority carrier diffusion lengths plotted as a function of applied dc bias for the p–n junction measurements of (c).

Figure 3c shows the spatial photocurrent along the length of a NW p–n junction device of Figure 3a for a series of applied dc biases from –1 V reverse bias to +1 V forward bias. The photocurrent does not show a strong bias dependence as the reverse bias is increased from 0 to –1 V. This behavior is consistent with the fact that the photocurrent is limited by the optical generation rate of the minority carriers in the neutral region and not by the depletion region width or electric field strength. The carriers generated in the depletion region and within one diffusion length will get swept across the junction due to the built-in electric field independent of the external applied reverse bias and the strength of the electric field. However, as the bias is increased in the forward direction from 0 to 1 V, the magnitude of the photocurrent decreases sharply implying that the current in forward bias is dominated by recombination in the depletion region. This conclusion is further supported by the greater than one ideality factor of the p–n diode. This enhanced recombination in forward bias decreases the overall photocurrent yield since minority carrier electrons (holes) will have a reduced probability of reaching the n-type (p-type) material which in turn decreases their

contribution to the photocurrent. Furthermore, the rate of exponential decay of the photocurrent and thus the minority carrier diffusion lengths do not vary appreciably in the range of applied dc bias (Figure 3d), consistent with minority carrier diffusion limited transport within the neutral region of the NW with a negligible drift component. We also observe that the position of the photocurrent peak shifts toward the p-doped segment as we tune the bias from forward to reverse direction. With increasing reverse bias, the geometric center of the depletion region moves further into the more lightly doped p region of the NW. This observation is consistent with the asymmetric p–n⁺ type junction for these NWs as determined by four point measurements and discussed earlier.

The results presented here for L_e^{eff} of $\sim 1.0 \mu\text{m}$ can be confirmed by comparing to an estimated L^{eff} determined from minority carrier lifetime measurements by Jung et al. for Si NW p–n junctions grown under the same conditions.³¹ From Jung et al.'s directly measured effective minority carrier lifetimes of $\sim 40\text{--}70 \text{ ns}$ for NW diameters $\sim 70 \text{ nm}$, we estimate a minority carrier diffusion length for electrons of $\sim 4 \mu\text{m}$,³² which is only moderately larger than observed here.

The observed electron and hole effective minority carrier diffusion lengths of $L_e^{\text{eff}} \approx 1.0 \mu\text{m}$ and $L_h^{\text{eff}} \approx 0.66 \mu\text{m}$ are much shorter compared to those observed in bulk Si with similar doping concentrations (i.e., $L_e \approx 300 \mu\text{m}$ and $L_h \approx 30 \mu\text{m}$)^{33,34} due to the close proximity of the surface for NWs. However our measured NW values are an order of magnitude longer than those previously reported in NWs of similar diameter (<100 nm).^{23,24} To compare our results with all prior reported minority carrier diffusion lengths on NWs of varying diameters and dopant concentrations, we have extracted the surface recombination velocity as a metric. The surface recombination velocity on NWs was first proposed by Allen et al. in the Supporting Information of ref 23 for relating the effective recombination lifetime, τ_{eff} to the bulk minority carrier lifetime, τ_b , where for a nanowire diameter d_{NW} and surface recombination velocity S the effective recombination lifetime is given by

$$1/\tau_{\text{eff}} = 1/\tau_b + 4S/d_{\text{NW}} \quad (1)$$

Substituting for τ_{eff} in eq 1 and ignoring the negligible contribution of the bulk recombination term (i.e., for $\tau_b \gg \tau_{\text{eff}}$), we get an expression for S in terms of L^{eff} as $S = d_{\text{NW}}D/(4(L^{\text{eff}})^2)$. The relative magnitude of the surface recombination velocity provides insight into the relative magnitude of the surface state density by relating the recombination efficiency of photogenerated electron (or holes) with the surface states. Table 1 compares reported L^{eff} and evaluated S values from the present and past published reports of nanowires and bulk crystalline silicon. For the small diameter NWs measured in refs 23 and 24, the minority carrier diffusion length and the surface recombination velocity are similar prior to surface passivation. However, after surface passivation with a-Si (ref 24), a minority carrier diffusion length was reported as being 7–11 times greater, whereas the surface recombination velocity decreased by 2 orders of magnitude which implies that the surface state density was dramatically reduced. In our case, we observe much longer minority carrier diffusion lengths and reduced surface recombination velocities (6×10^2 to 4×10^3 cm/s) without any additional surface passivation, suggesting that our as-grown NWs are well passivated and have a low surface state density. Also, in comparison to the as-grown large diameter (1–2 μm) Si microwires which were grown with SiCl_4 source gases at higher temperatures ($\sim 1000 \text{ }^\circ\text{C}$) and with both Au and Cu as the growth catalysts, the effective minority carrier diffusion length is comparable to our values for much smaller diameter Si NWs before passivation. In fact the surface recombination velocity in ref 26 is 2 orders of magnitude larger than that of our Si NWs prior to passivation. The above results suggest that the density of surface states in our in situ doped p–n junction NWs grown in a cold wall reactor is much reduced from that of previous reports where in all cases the NWs were grown in hot-wall reactor systems. The improved surface recombination velocities found here may result from reduced precursor reactions or deposition on the NW sidewalls resulting in a lower density of recombination centers at the NW surface.

The submission that the Si NWs in the present study, which were synthesized with a cold-wall CVD reactor, have a reduced surface state density is further supported by measuring the effective minority carrier diffusion lengths with and without the presence of a background illumination. Results for the effective minority carrier diffusion lengths of a NW at 0 V are shown in Figure 4 for the conditions with and without broad area dc background illumination in the low-injection limit provided by

Table 1. Comparison of Experimental Results on Measuring the Minority Carrier Diffusion Length in Si Nanowires

Si NWs	VLS catalyst	device structure	NW diameter d (nm)	technique	N_A/cm^3	N_D/cm^3	before passivation			after passivation		
							L^{eff} (nm)	S (cm/s)	ref	L^{eff} (nm)	S (cm/s)	ref
	Au	Au/n-Si/Au Schottky	small d NWs (≤ 100 nm)	EBIC	1×10^{18}	1×10^{19}	$\sim 20\text{--}80 (L_b)$	$\sim 1 \times 10^5$	23	$\sim 250\text{--}400 (L_e)$	$\sim 4 \times 10^3$	23
	Au	Au/p-Si/Au Schottky			2×10^{16}	2×10^{18}	$\sim 25\text{--}100 (L_e)$	$\sim 3 \times 10^5$	24			our work
	Au	Ni/n-Si/p-Si/Ni axial pn junctions					$\sim 660 (L_h)$	$\sim 4 \times 10^3$				
	Au	Al/n-Si/Al Schottky	large d microwires (1–2 μm)	SPCM	1×10^{17}	1×10^{17}	$\sim 1000 (L_e)$	$\sim 6 \times 10^2$				25
	Cu	Al/p-Si/n-Si/Al ex situ doped pn junctions			1×10^{17}	1×10^{17}	$\sim 2000 (L_b)$	$\sim 1 \times 10^3$				26
c-Si		bulk Si		EBIC	2×10^{16}	2×10^{18}	$\leq 500 (L_e)$	$> 4 \times 10^5$			$\geq 30\,000 (L_e)$	33 and 34
							$\sim 50\,000 (L_b)$	< 1				
							$\sim 250\,000 (L_e)$					

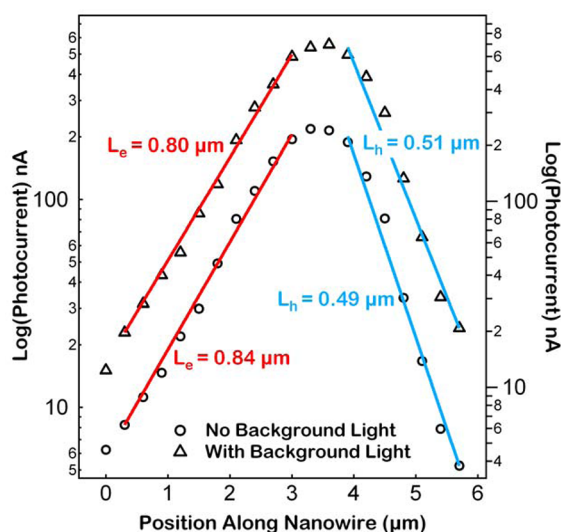


Figure 4. Semi log plots of photocurrent profiles of a Si nanowire p–n junction measured at 0 V without background illumination (open circles) and with background illumination (open triangles). The fit to the exponential decay of the photocurrent gives the effective electron and hole diffusion lengths.

a separate laser of $\lambda = 900$ nm. A similar experiment was performed by Putnam et al.²⁷ on large diameter ($d \approx 2.0$ μm) Si microwires where effective diffusion lengths increased from ≤ 0.7 μm to ~ 10 μm in the presence of broad area illumination. This increase was attributed to increased surface passivation due to the filling of surface states by the photogenerated carriers created by the background light. In contrast, we find that there is very little change in the effective minority carrier diffusion lengths measured with and without the background light. This result supports the view that the present as-grown NWs have significantly fewer surface states. In addition, in another report³⁵ it was determined using TEM that InAs NWs grown with a cold-wall system had high crystalline quality and much reduced defect density as compared to InAs NWs grown with a hot-wall reactor. However, to truly understand the variations in surface recombination for NWs due to subtle variations in the growth conditions such as for different types of reactors (hot wall versus cold wall), growth temperatures, and partial pressures, a quantitative comparison across NWs grown under different conditions from different laboratories is required and beyond the scope of this study.

In summary, surface recombination provides the major limitation for achieving long effective minority carrier diffusion lengths in nanowires and thus control of surface quality is of key importance in achieving efficient photocurrent response essential for solar cell applications. We have reported here effective minority carrier diffusion lengths for single crystalline Si nanowire p–n junctions which are an order of magnitude larger than previously reported for as-grown small diameter nanowires (< 100 nm). These devices show a high internal quantum efficiency of $\sim 50\%$, consistent with low surface recombination velocities compared to those found in previous as-grown nanowire and microwire studies. These observations of long effective minority carrier diffusion lengths in our nanowires suggests that the surface state density is lower in comparison with previous reports and are promising for more efficient future photovoltaic device applications.

■ ASSOCIATED CONTENT

Supporting Information

Control experiments to verify the observed large values of L^{eff} . This material is available free of charge via the Internet at <http://pubs.acs.org>.

■ AUTHOR INFORMATION

Corresponding Author

*E-mail: amohite@lanl.gov; picraux@lanl.gov; htoon@lanl.gov.

Present Addresses

^{||}Environmental Molecular Science Laboratory, Pacific Northwest National Laboratory, Richland, WA 99352.

[†]School of Electrical and Computer Engineering, Georgia Institute of Technology, Atlanta, GA 30332.

Notes

The authors declare no competing financial interest.

■ ACKNOWLEDGMENTS

We thank John Baldwin from the Center for Integrated Nanotechnologies (CINT) at Los Alamos National Laboratory (LANL) for his help in preparing the growth substrates needed for the nanowire synthesis. This work was performed, in part, at CINT, a U.S. Department of Energy, Office of Basic Energy Sciences user facility. The research was funded in part by the Laboratory Directed Research and Development Program and by CINT at LANL, an affirmative action equal opportunity employer operated by Los Alamos National Security, LLC, for the National Nuclear Security Administration of the U.S. Department of Energy under contract DE-AC52-06NA25396.

■ REFERENCES

- (1) Shah, A.; Torres, P.; Tscharnner, R.; Wyrsh, N.; Keppner, H. *Science* **1999**, *285* (5428), 692–698.
- (2) Brendel, R. *Introduction, in Thin-Film Crystalline Silicon Solar Cells: Physics and Technology*; Wiley: New York, 2003.
- (3) Lewis, N. S. *Science* **2007**, *315* (5813), 798–801.
- (4) Boettcher, S. W.; Spurgeon, J. M.; Putnam, M. C.; Warren, E. L.; Turner-Evans, D. B.; Kelzenberg, M. D.; Maiolo, J. R.; Atwater, H. A.; Lewis, N. S. *Science* **2010**, *327* (5962), 185–187.
- (5) Goodey, A. P.; Eichfeld, S. M.; Lew, K. K.; Redwing, J. M.; Mallouk, T. E. *J. Am. Chem. Soc.* **2007**, *129* (41), 12344.
- (6) Gunawan, O.; Wang, K.; Fallahzad, B.; Zhang, Y.; Tutuc, E.; Guha, S. *Prog. Photovoltaics* **2011**, *19* (3), 307–312.
- (7) Kendrick, C. E.; Yoon, H. P.; Yuwen, Y. A.; Barber, G. D.; Shen, H.; Mallouk, T. E.; Dickey, E. C.; Mayer, T. S.; Redwing, J. M. *Appl. Phys. Lett.* **2010**, *97* (14), 143108.
- (8) Maiolo, J. R.; Kayes, B. M.; Filler, M. A.; Putnam, M. C.; Kelzenberg, M. D.; Atwater, H. A.; Lewis, N. S. *J. Am. Chem. Soc.* **2007**, *129* (41), 12346.
- (9) Putnam, M. C.; Boettcher, S. W.; Kelzenberg, M. D.; Turner-Evans, D. B.; Spurgeon, J. M.; Warren, E. L.; Briggs, R. M.; Lewis, N. S.; Atwater, H. A. *Energy Environ. Sci.* **2010**, *3* (8), 1037–1041.
- (10) Stelzner, T.; Pietsch, M.; Andra, G.; Falk, F.; Ose, E.; Christiansen, S. *Nanotechnology* **2008**, *19* (29).
- (11) Tsakalacos, L.; Balch, J.; Fronheiser, J.; Korevaar, B. A.; Sulima, O.; Rand, J. *Appl. Phys. Lett.* **2007**, *91* (23).
- (12) Picraux, S. T.; Yoo, J.; Campbell, I. H.; Dayeh, S. A.; Perea, D. E. *Semiconductor Nanowires for Solar Cells. In Semiconductor nanostructures for optoelectronic devices*; Springer: New York, 2011.
- (13) Wagner, R. S.; Ellis, W. C., *Appl. Phys. Lett.* **1964**, *4* (5), 89–8.
- (14) Cui, Y.; Lauhon, L. J.; Gudiksen, M. S.; Wang, J.; Lieber, C. M., *Diameter-controlled synthesis of single-crystal silicon nanowires*. *AIP*: 2001; Vol. 78, p 2214–2216.

- (15) Kelzenberg, M. D.; Boettcher, S. W.; Petykiewicz, J. A.; Turner-Evans, D. B.; Putnam, M. C.; Warren, E. L.; Spurgeon, J. M.; Briggs, R. M.; Lewis, N. S.; Atwater, H. A. *Nat. Mater.* **2010**, *9* (3), 239–244.
- (16) Kempa, T. J.; Tian, B.; Kim, D. R.; Hu, J.; Zheng, X.; Lieber, C. M. *Nano Lett.* **2008**, *8* (10), 3456–3460.
- (17) Gudiksen, M. S.; Lauthon, L. J.; Wang, J.; Smith, D. C.; Lieber, C. M. *Nature* **2002**, *415* (6872), 617–620.
- (18) Tian, B.; Zheng, X.; Kempa, T. J.; Fang, Y.; Yu, N.; Yu, G.; Huang, J.; Lieber, C. M. *Nature* **2007**, *449* (7164), 885–889.
- (19) Cui, Y.; Duan, X.; Hu, J.; Lieber, C. M. *J. Phys. Chem. B* **2000**, *104* (22), 5213–5216.
- (20) Kelzenberg, M. D.; Putnam, M. C.; Turner-Evans, D. B.; Lewis, N. S.; Atwater, H. A. In *Predicted efficiency of Si wire array solar cells*; Photovoltaic Specialists Conference (PVSC), 2009 34th IEEE; 2009; pp 001948-001953.
- (21) Bullis, W. M. *Solid State Electron.* **1966**, *9* (2), 143.
- (22) Sze, S. M. *Physics of Semiconductor devices*; Wiley-Interscience: New York, 1969; p xiv–812.
- (23) Allen, J. E.; Hemesath, E. R.; Perea, D. E.; Lensch-Falk, J. L.; Li, Z. Y.; Yin, F.; Gass, M. H.; Wang, P.; Bleloch, A. L.; Palmer, R. E.; Lauthon, L. J. *Nat. Nanotechnol.* **2008**, *3* (3), 168–173.
- (24) Dan, Y.; Seo, K.; Takei, K.; Meza, J. H.; Javey, A.; Crozier, K. B. *Nano Lett.* **2011**, *11* (6), 2527–2532.
- (25) Kelzenberg, M. D.; Turner-Evans, D. B.; Kayes, B. M.; Filler, M. A.; Putnam, M. C.; Lewis, N. S.; Atwater, H. A. *Nano Lett.* **2008**, *8* (2), 710–714.
- (26) Kelzenberg, M. D.; Turner-Evans, D. B.; Putnam, M. C.; Boettcher, S. W.; Briggs, R. M.; Baek, J. Y.; Lewis, N. S.; Atwater, H. A. *Energy Environ. Sci.* **2011**, *4* (3), 866–871.
- (27) Putnam, M. C.; Turner-Evans, D. B.; Kelzenberg, M. D.; Boettcher, S. W.; Lewis, N. S.; Atwater, H. A. *Appl. Phys. Lett.* **2009**, *95*, 16.
- (28) Picraux, S. T.; D., S.; Manandhar, P.; Perea, D. E.; Choi, S. G. *J. Mater.* **2010**, *62* (4), 35.
- (29) Gu, Y.; Romankiewicz, J. P.; David, J. K.; Lensch, J. L.; Lauthon, L. J. *Nano Lett.* **2006**, *6* (5), 948–952.
- (30) It should be noted that in all of the devices Ni was used to make contacts to the NWs. Ni typically is known to form Schottky contact to n-type Si NWs, but the Schottky barrier height is strongly dependent on the local doping concentration. In our study we found that out of 20 two terminal devices fabricated using Ni as the metal contact only three devices showed lower photocurrent at both the p and n contacts (ohmic) while for other devices the n segment formed a Schottky contact to Ni.
- (31) Jung, Y.; Vacic, A.; Perea, D. E.; Picraux, S. T.; Reed, M. A. *Adv. Mater.* **2011**.
- (32) A diffusion constant of $D_e \approx 3.38 \text{ cm}^2/\text{s}$ and $D_h \approx 9.8 \text{ cm}^2/\text{s}$ was calculated using bulk mobilities for Si at the doping concentrations estimated from resistivity measurements.
- (33) del Alamo, J. A.; Swanson, R. M. *Solid State Electron.* **1987**, *30* (11), 1127–1136.
- (34) Tyagi, M. S.; Van Overstraeten, R. *Solid State Electron.* **1983**, *26* (6), 577–597.
- (35) Schroer, M. D.; Xu, S. Y.; Bergman, A. M.; Petta, J. R. *Rev. Sci. Instrum.* **2010**, *81* (2).